HOSTED BY

ELSEVIER

Available online at www.sciencedirect.com

ScienceDirect

Journal of Magnesium and Alloys 5 (2017) 225–230
www.elsevier.com/journals/journal-of-magnesium-and-alloys/2213-9567

Full Length Article

Stress–rupture measurements of cast magnesium strengthened by in-situ production of ceramic particles

Nagaraj M. Chelliah [a,b], Sudarshan [a], Lisa Kraemer [a,c], Harpreet Singh [b,*], M.K. Surappa [d], Rishi Raj [a]

[a] *Department of Mechanical Engineering, University of Colorado Boulder, Boulder, CO 80302, USA*
[b] *Department of Mechanical Engineering, Indian Institute of Technology, Ropar 140001, India*
[c] *Erich Schmid Institute of Material Science, Austrian Academy of Sciences, Leoben, A-8700, Austria*
[d] *Department of Materials Engineering, Indian Institute of Science, Bangalore 560012, India*

Received 21 November 2016; revised 7 April 2017; accepted 18 April 2017

Available online 17 May 2017

Abstract

We have introduced a polymer precursor into molten magnesium and then in-situ pyrolyzed to produce castings of metal matrix composites (P-MMCs) containing silicon-carbonitride (SiCNO) ceramic particles. Stress-rupture measurements of as-cast P-MMCs was performed at 350 °C ($0.69T_M$) to 450 °C ($0.78T_M$) under dead load condition corresponding to tensile stress of 2.5 MPa to 20 MPa. The time-to-fracture data were analyzed using the classical Monkman–Grant equation. The time-to-fracture is thermally activated and follows a power-law stress exponent exhibiting dislocation creep. Fractography analysis revealed that while pure magnesium appears to fracture by dislocation slip, the P-MMCs fail from the nucleation and growth of voids at the grain boundaries.

Keywords: Stress-rupture; Polymer derived ceramics; Magnesium; Dispersion strengthened alloys; High temperature; Light-weight materials

1. Introduction

Mg-alloys are the potential candidate materials to be employed in transport applications because of the combination of high specific strength and enhanced fuel efficiency [1,2]. However, precipitation hardened Mg-alloys lose their viability at elevated temperatures owing to the Oswald ripening mechanism [3]. Hence, dispersion strengthened metal matrix composites (MMCs) are preferred choice of high temperature material design as ceramic particles do not coarsen especially at elevated temperature regimes [4,5]. The creep properties and creep mechanisms of MMCs are mainly determined by being able to impede the glide or climb motion of dislocations at elevated temperature, which depends greatly on the particle size and volume fraction of the reinforced ceramic particles. As Orowan strength inversely scales with size of reinforced particles, nanoscale ceramic particles are needed to impede dislocation motion for any meaningful increase in the creep strength of MMCs. At high volume fractions where the metal channels between the particles may be narrower than the average spacing between the dislocations; their movement is geometrically constrained [6]. The γ–γ' single crystal super alloys are a sterling example of how high volume fractions of the γ' phase can be employed to achieve creep resistance at elevated temperatures [6]. Solidification processing of MMCs having higher volume fraction of nanoscale ceramic particles is often a challenging task owing to particle agglomeration caused by Van der Waals force of attraction. Therefore, dilute volume fractions (1.0 to 2.5 vol %) of nanoscale ceramic particles are most often preferred in metal matrix nanocomposites (MMNCs) [7]. Most of the technical challenges (non-uniformity of particle distribution, poor wettability and weak interfaces) in solidification processing of MMCs can be greatly reduced by adopting in-situ composite approach by which ceramic particles are generated within the molten state via chemical reaction between the added precursor and the host metal. Investigators at the University of Colorado and the Indian Institute of Science have been collaborating to explore the possibility of enhancing the creep resistance performance in polymer-derived metal matrix composites (P-MMCs) by utilizing the in-situ pyrolysis approach [8–14].

* Corresponding author. Department of Mechanical Engineering, Indian Institute of Technology, Ropar 140001, India. Fax: +91 1881 223395.
E-mail address: harpreetsingh@iitrpr.ac.in (H. Singh).

http://dx.doi.org/10.1016/j.jma.2017.04.002

Noteworthy feature of this in-situ pyrolysis approach is that no chemical reaction between polymer precursor and the host Mg is required to produce ceramic particles as polymer contains all the constituents of ceramic phases within organic molecules itself [8,9]. The in-situ pyrolysis is a highly reactive process, accompanied by the evolution of hydrogen, which disperses the ceramic phase into nanoscale or sub-micron constituents [8,9]. Nanoscale particles of **polymer derived ceramic (PDCs)** dispersed into metals can be expected to impede dislocation motion and resist coarsening at high temperatures, there by holding the promise of a new genre of polymer-derived metal matrix composites (P-MMCs).

Ferkel et al. [15] reinforced the Mg matrix with 3 vol% of SiC nanoparticles via ball milling process and achieved the higher flow stress and lower creep rate as compared to pure Mg. Labib et al. [16] studied the impression creep of extruded Mg-SiCp composites and observed that dislocation creep as a dominant creep mechanism with improved creep performance. Despite the fact that several researchers investigated the creep and mechanical properties of MMCs [15–18], less attention has been paid to explore the stress-rupture behavior of in-situ processed MMCs. In the present study, we have made an attempt to measure the stress-rupture properties of in-situ magnesium metal matrix composites (P-MMCs) containing polymer derived SiCNO dispersoids in the temperature range of 350–450 °C.

2. Experimental procedures

2.1. In-situ processing

Pure magnesium (99.9%) and a polysilazane precursor (Ceraset, KiON Defense Technologies), were selected as the starting materials. The processing methodology essentially comprises of two fundamental steps namely, (i) cross-linking the liquid precursor, at about 350 °C, which yields a hard and brittle organic material followed by ball-milling process to produce micron-sized polymer particles (mean particle size is in the range of 1 to 50 μm), and (ii) dispersing the ceramic particles via in-situ pyrolysis of cross-linked polymer particles within molten Mg at about 800 °C followed by solidification [8,9]. In-situ pyrolysis releases hydrogen gas and other organic based volatile compounds to leave behind the sub-micron/nano-sized thermally stable SiCNO ceramic dispersoids in the magnesium matrix [8,9]. The amount of cross-linked polymer added to the melt was adjusted to achieve an estimated volume fraction of 2.5% of the amorphous SiCNO ceramic phase assuming a density of ~2 g cm^{-3} for the ceramic and an 80 wt% yield from the polymer into the ceramic state [19].

A sketch of the casting set up is shown in Fig. 1. The castings were made by the stir-casting technique inside a glove box within which the oxygen level was maintained to below 1 ppm. 200 gm of magnesium blocks was heated to a temperature of 700 °C using electrical resistance furnace. A mechanical impeller was rotated at 600 rpm in order to create a vortex within the melt. A funnel placed close to the surface of the melt was used to channel down the cross-linked polymer into vortex of the molten metal. After the polymer addition, the temperature was

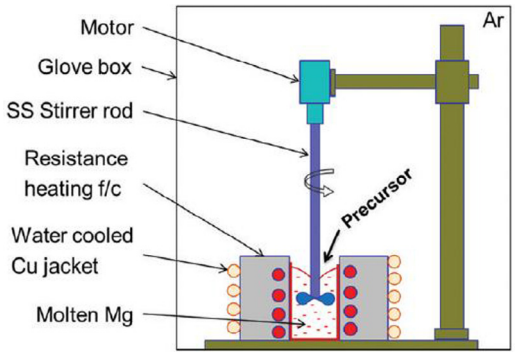

Fig. 1. Schematic diagram for casting set up with mechanical stirring. The set is placed inside a glove box with oxygen levels of less than 1 ppm.

increased to 800 °C to complete the conversion of polymer into ceramic phase. The stirring action was continued for another 15 min to achieve the homogenous dispersion of PDC particles throughout the melt. Finally, the molten slurry was poured into a preheated (at a temperature of 100 °C) split-cast iron mold to produce castings. For comparative purposes, pure magnesium was also fabricated by a similar control. The test coupons including flat dog-bone specimens were machined out from the castings. The flat dog-bone specimens had a gauge length of 30 mm, a width of 6 mm and a thickness of 3 mm. These test coupons were used for microstructural analysis and stress-rupture testing.

2.2. Stress-rupture tests

Stress-rupture behavior of the fabricated pure Mg and composites was investigated by home-built high temperature testing instrument as shown in Fig. 2. Stress-rupture data were obtained at a temperature in the range of 350 °C to 450 °C under dead loading conditions corresponding to tensile stresses of 2.5 MPa to 20 MPa in accordance with the ASTM standards [20]. Temperature controller was used to maintain the constant temperature throughout the specimen using an electrically

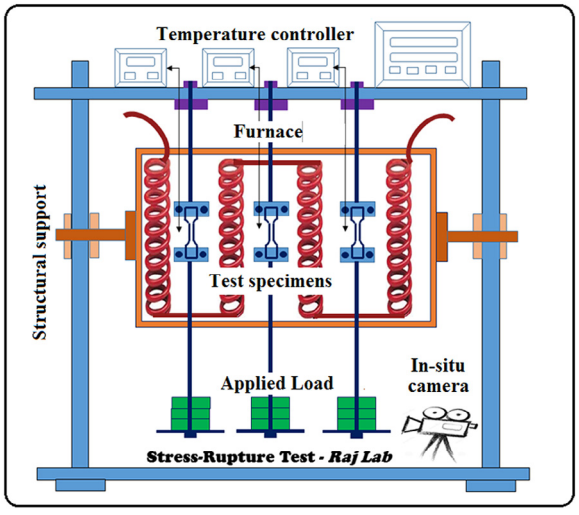

Fig. 2. Schematic diagram of home-built stress-rupture testing configuration.

resistant heating filament. A video camera was installed to monitor the positional change of dead load such that failure of ruptured specimen can be tracked continuously in order to determine the time to fracture in the stress-ruptured specimens.

2.3. Material characterization

The microstructures and fractography of as-cast and stress-ruptured composites are characterized using scanning electron microscope (Sirion, Model: VL3FEG). Spot chemistries for Si, C, N, Mg and O are characterized by energy-dispersive spectroscopy (EDS). The size and morphology of nano-sized SiCNO particles in as-cast composite are analyzed by transmission electron microscope.

3. Results and discussion

Fig. 3 shows the microstructures of polymer-derived magnesium matrix composites at different magnifications. EDS analysis on the PDC particles revealed the presence of Si, C, N and O (Fig. 3(a)). The average grain size of the fabricated P-MMCs is found to be in the range of 40–60 μm, while it was 400–450 μm for the case of unreinforced pure Mg specimen. The grain size reduction of as-cast P-MMCs could be attributed to two primary factors; (i) availability of heterogeneous nucleation sites (SiCNO and Mg_2Si phases) and (ii) restricting grain growth during solidification [8,9,13]. It can be observed that most of the PDC particles segregated at the grain boundaries as shown in Fig. 3(a) through Fig. 3(c). This may be ascribed to the rejection of PDC particles by solidification front during casting process [8,9,13]. The formation of Mg_2Si phase (marked as A) is evident in the fabricated P-MMC as depicted in Fig. 3(a). This happens because of the chemical reaction between the added polymer precursor and the host magnesium [8,9,13]. The morphology of PDC particles showed two distinct features (round or spherical and rod-like or platelet types), which is almost similar as observed in our earlier work [7,8]. TEM micrograph confirms the existence of nano-sized SiCNO ceramic particles (mean particle size is in the range of 200–500 nm) within the grain matrix of magnesium. Line profile chemical analysis confirmed the presence of Si-atoms in silicon oxy-carbonitride (SiCNO) ceramic particles as seen in Fig. 3(d). One of them has a lenticular shape which is typical feature of an amorphous material at a grain boundary, as observed in the dispersion of silica-glass particles in copper produced by internal oxidation [21].

The experimental data for the time-to-fracture as a function of stress and temperature were analyzed using the classical Monkman–Grant equation as follows [22]:

$$\dot{\varepsilon} t_f = \varepsilon_{MG} \tag{1}$$

where $\dot{\varepsilon}$ is the *steady state* strain rate, t_f is the time to fracture, and ε_{MG} is related to the Monkman–Grant strain. The Monkman–Grant strain is equal to the strain accumulated during the steady-state creep regime of the experiments, which produces uniform deformation in the specimen gauge length. The values for ε_{MG} for all specimens were determined from the reduction in the cross section area of the gauge section using the equation;

$$\varepsilon_{MG} = \ln\left(\frac{A_o}{A_f}\right) \tag{2}$$

where A_o is the initial cross section, and A_f is the final cross section of the stress-ruptured samples. Notice that the cross section area was measured away from the fracture surface, where the deformation had not been localized. The steady-state

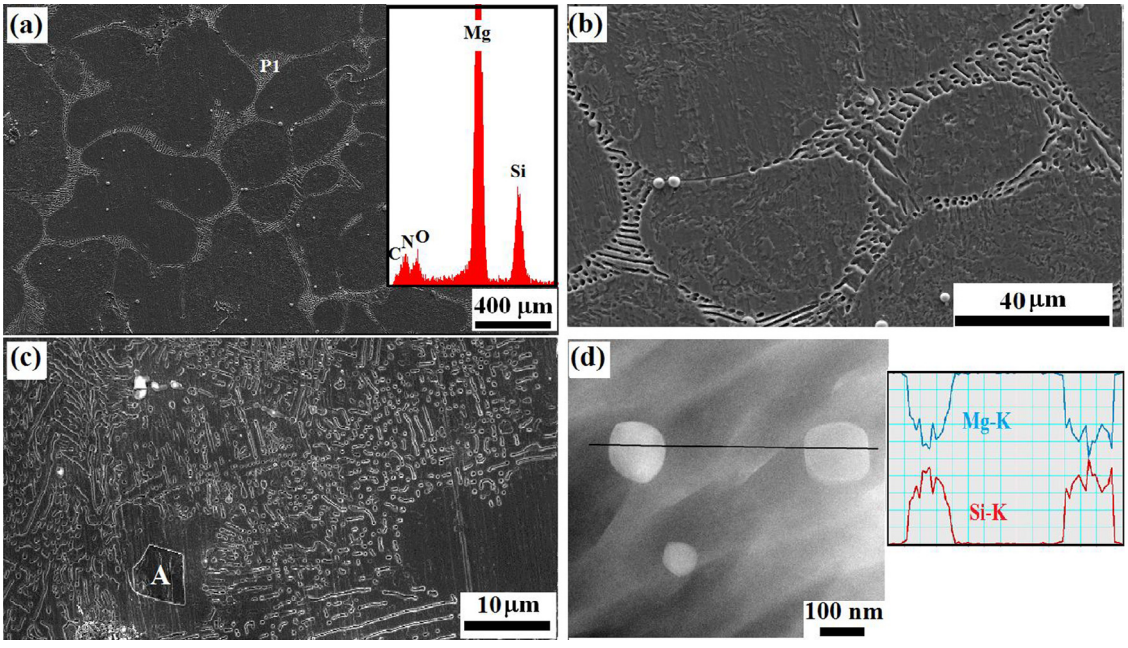

Fig. 3. (a) Microstructure of Mg matrix composites with Energy Dispersive Spectrum (b) and(c) Microstructures showing the grain boundary segregation of SiCNO particles along with particle morphology, and (d) TEM micrograph depicting the existence of nanoscale SiCNO particles in the magnesium matrix.

creep strain rate $(\dot{\varepsilon})$ was then determined by inserting the experimental values for ε_{MG} and t_f into Eq. (1).

Toaz et al. [23] reported the deformation mechanism map for Mg polycrystal (mean grain size of 100 μm) where one creep mechanism dominates over the others depending upon temperature and applied stress. Although deformation mechanism map [24] is for primarily metals or alloys; still it provide a framework for the design of engineering materials such as metal matrix composites especially with a dilute volume fraction of ceramic particles. Stress-rupture data span from $0.69T_m$ to $0.78T_m$ under applied stress (σ) of 10^{-4} to 10^{-3} (σ/G) where G is the shear modulus of the composites. As verified from Ref [24], it is predicted that the high temperature power-law creep may control the stress-rupture behavior of fabricated Mg matrix composites for temperature-stress ranges covered in the present study. We have assumed that steady-state creep strain rate in Eq. (1) is expected to obey the power-law creep behavior given by the following equation [24]:

$$\dot{\varepsilon} = A\sigma^n exp^{\left[\frac{-Q}{RT}\right]} \tag{3}$$

where, σ is the applied tensile stress, $\boldsymbol{n}$ is the power-law stress exponent, R is gas constant, Q is the activation energy, R is gas constant, $\boldsymbol{T}$ is temperature in K, and $\boldsymbol{A}$ is a materials-specific parameter that depends on the microstructure. The value of $\boldsymbol{n}$ in Eqn (3) was determined by plotting the logarithm of the strain rate versus the logarithm of the stress, at a given temperature. The slope of these graphs yields the value for $\boldsymbol{n}$. The value for the activation energy was obtained by combining Eqn (1) with Eqn (3) into the following form:

$$\mathrm{Log}_{10}\left[\frac{t_f}{\varepsilon_{MG}} exp^{\left(\frac{-Q}{RT}\right)}\right] = -\mathrm{Log}_{10}(A) - n\mathrm{Log}_{10}(\sigma) \tag{4}$$

The experimental values of t_f, ε_{MG}, and σ together with the values for n as estimated above, were plotted in a log-log plot with different values of Q.

The stress-rupture data for all investigated specimens are given in Table 1. It shows the nine results for pure-Mg and a similar number for the P-MMC specimens. Three specimens were prepared and tested for each of the nine results. As seen in Table 1, the time-to-fracture ranged from just a few minutes (0.03 h) at 450 °C and 7.5 MPa in pure Mg, to 432 h at 400 °C and 5 MPa in the P-MMCs. The time-to-fracture for the composites is lengthened by three orders of magnitude relative to pure magnesium. Several microstructural factors are believed to be the main reasons for such enhancement in stress-rupture performance of the fabricated P-MMCs. They include (i) Orowan strengthening by the presence of nano-sized PDC particles in the magnesium matrix, (ii) improved interfacial bonding strength between the PDC particles and the magnesium matrix, and (iii) higher probability of arresting the grain boundary sliding movement as well as grain boundary growth owing to the segregation of PDC particles at the grain boundaries.

Vagarali et al. [25] investigated the creep behavior of Mg polycrystal over the temperature range from 200 to 547 °C by isothermal creep testing. They determined that the power-law stress exponent "n" is 6 for dislocation creep, and activation energy is found to be stress dependent (140 + [295/σ] kJ/mol). The graphs for stress-rupture data at 450 °C and 350 °C are shown in Fig. 4(a) (the data for 400 °C yielded similar slope but is not included in the figure for clarity). These plots yield $\boldsymbol{n = 6–7}$ which is consistent with the values reported by Vagarali et al. [25]. This suggests that the mechanism of power-law creep is controlled by dislocation assisted creep and similar values for pure Mg and the composites represent creep mechanism remain the same in both of these materials. The best fit to the data for both pure Mg and the composite are shown in Fig. 4(b); they yield $Q = 215\ kJmol^{-1}$ for Mg and $Q = 190\ kJmol^{-1}$ for the composite, again in agreement with the value reported in the literature [26]. The modification of MG equation has been suggested by several researchers to understand the role played by reinforced ceramic particles in the stress-rupture behavior of the MMCs [16,27,28]. However, no such modification is required as stress-rupture data fits well with Monkman–Grant equation in the present work (see Fig. 4(b)). It is well-documented that power-law creep equation applies to the composites, even though the voids at the grain boundaries grow by diffusional mechanisms. This is because of their growth rate must be accommodated by matrix deformation, which eventually then becomes the rate controlling process in the fracture mechanism of the composites [29]. The unusual higher values of n and Q in pure Mg relative to P-MMCs may be attributed to extensive cross-slip of dislocation from basal to non-basal planes at elevated temperatures [26]. The existence of large

Table 1
Summary of stress-rupture data for the present work.

T °C	Pure Mg				P-MMC			
	Stress (MPa)	Time to rupture (hr)	MG strain	Creep rate (s^{-1})	Stress (MPa)	Time to rupture (hr)	MG strain	Creep rate (s^{-1})
450	2.5	155 ± 6.8	0.24 ± 0.02	4.8×10^{-7}	5	25.9 ± 1	0.029 ± 0.001	3.1×10^{-7}
450	5	0.74 ± 0.3	0.25 ± 0.02	9.4×10^{-5}	7.5	8.2 ± 1.4	0.031 ± 0.005	1.15×10^{-6}
450	7.5	0.03 ± 0.01	0.26 ± 0.04	2.4×10^{-3}	10	0.7 ± 0.06	0.040 ± 0.003	1.55×10^{-5}
400	5	24.1 ± 3.8	0.24 ± 0.09	3.0×10^{-6}	5	432 ± 3.0	0.031 ± 0.002	1.9×10^{-8}
400	7.5	0.6 ± 0.15	0.25 ± 0.01	1.1×10^{-4}	10	8.4 ± 0.2	0.024 ± 0.005	7.97×10^{-7}
400	10	0.1 + 0.01	0.26 ± 0.06	7.2×10^{-4}	15	0.5 ± 0.05	0.039 ± 0.004	2.18×10^{-5}
350	7.5	9.1 ± 2.04	0.24 ± 0.01	7.5×10^{-6}	10	107 ± 10	0.036 ± 0.003	9.4×10^{-8}
350	10	4.7 ± 0.14	0.25 ± 0.02	1.5×10^{-5}	15	12.6 ± 4.1	0.028 ± 0.009	6.1×10^{-7}
350	15	0.2 + 0.05	0.26 ± 0.01	3.5×10^{-4}	20	0.9 ± 0.08	0.032 ± 0.002	1.01×10^{-5}

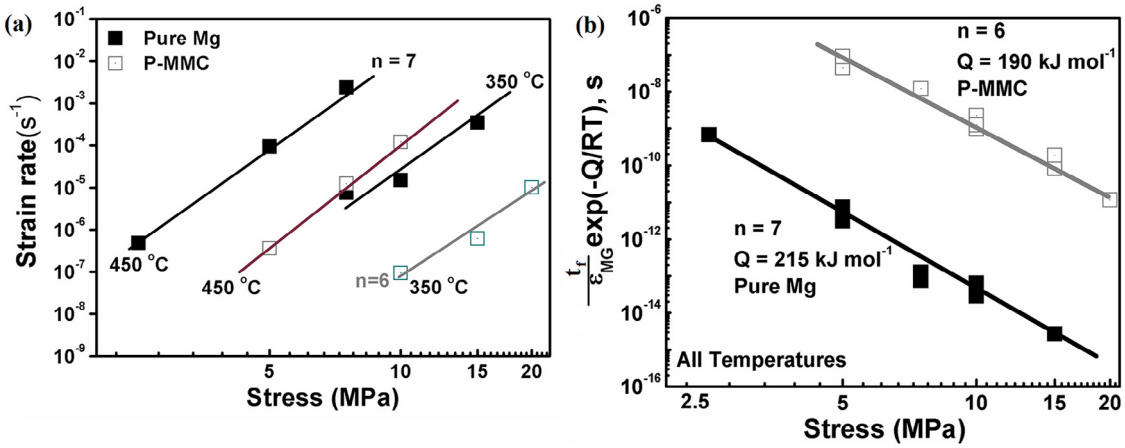

Fig. 4. a) Logarithmic plot of strain rate vs. applied stress, and (b) Logarithmic plot to determine the apparent activation energy (Q).

amount of slip bands in stress-ruptured pure Mg as seen in Fig. 5(a) confirms this extensive cross-slip activity.

It is reported that cavities often nucleate at the grain boundaries, and grow as deformation progresses, causing fracture when a certain limit of strain/cavities is attained [16]. For the case of P-MMCs, cavity formation is expected to occur usually at the metal-ceramic interface. It is well-known that in-situ MMCs consist of ultra fine-sized and thermodynamically stable ceramic particles, clean and unoxidized ceramic-metal interfaces with high interfacial strength, due to improved wettability [30]. This is also true for the fabricated in-situ Mg-based P-MMCs in the present work. In fact, TEM micrograph confirmed the existence of clean interface between PDC particles and the magnesium matrix as shown in Fig. 3(d). The strain to fracture for pure Mg was 25% but only 3.5 ± 0.5% for the dispersion strengthened P-MMCs, which is typical of intergranular embrittlement at elevated temperatures arising from the nucleation and growth of voids at the grain boundaries [31,32]. This means that matrix deformation is certainly limited by the presence of PDC particles in the stress-ruptured P-MMCs. The micrographs of the fracture surfaces in Fig. 5(a) contrast the transgranular fracture in pure magnesium, also reported by Tegart [26], with intergranular fracture in dispersion strengthened P-MMCs as shown in Fig. 5(b). The fracture morphology shows a transition from transgranular failure in pure magnesium to intergranular fracture by cavitation in the composite as verified in Fig. 5. While pure Mg fails by transgranular fracture because of extensive cross-slip activities, P-MMCs exhibit intergranular fracture mode owing to to nucleation and growth of cavities at grain boundaries.

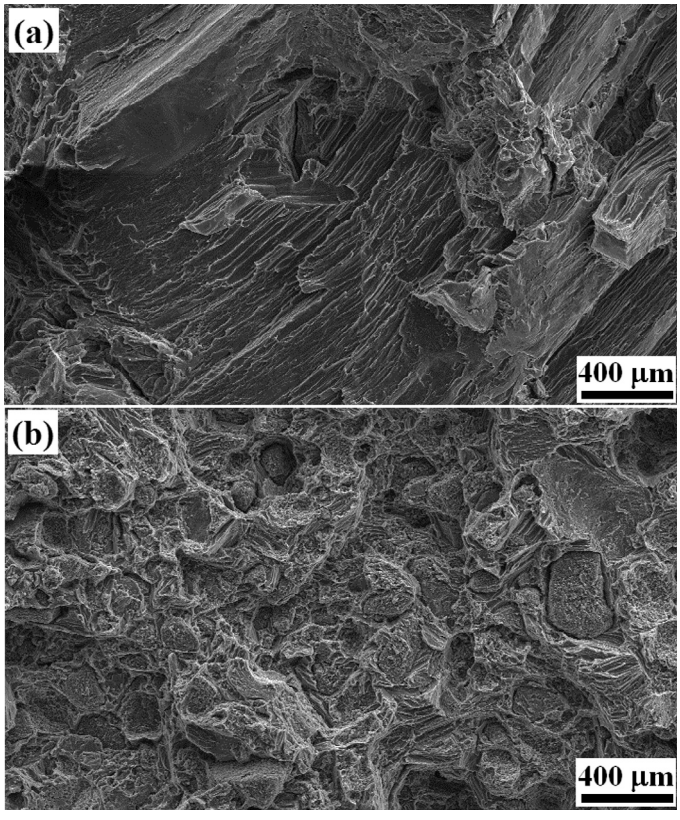

Fig. 5. Fracture surfaces from stress-rupture experiments showing the transition from transgranular fracture in pure Mg to intergranular fracture in P-MMCs.

After performing the comparative analysis as seen in Table 2, the creep resistance performance of the fabricated P-MMCs appears to be more or less better than that of creep resistant AE44 Mg-alloys and other Mg/n-SiC composites reported in Refs [15,33,34]. In summary, the trend in stress-rupture data illustrates clearly that polymer derived SiCNO ceramic phase provides a higher resistance to grain matrix growth and grain boundary sliding during creep deformation within P-MMCs, where as pure Mg does not hold this capability at elevated temperatures. This also confirms the non-coarsening properties of the polymer derived ceramic phase. It is expected that stress-rupture performance of P-MMCs described here may encourage research communities to develop variety of P-MMCs with other commercial Mg-alloy castings in the near future. However, care must be taken to control the dispersion of the PDCs in the commercial Mg-alloy melt.

4. Conclusions

1. Stress-rupture behavior of polymer-derived MMCs obeys power-law creep with stress exponent n of 6 exhibiting

Table 2
Comparative analysis on the stress-rupture performance of P-MMCs.

Material	Creep strain	Creep rate (s^{-1})	Time to rupture (hr)	References
Pure Mg	0.25 @ 400 °C, 5 MPa	3.0×10^{-6}	24.1 ± 3.1	Present work
Mg-2.5vol% SiCN (P-MMC)	0.032@ 400 °C, 5 MPa	1.9×10^{-8}	432.3 ± 4.1	Present work
Mg-4Al-4RE alloy	0.30 @ 200 C, 60 MPa	5.72×10^{-10}	120	Keilbus et al. [33]
Mg-3.5 vol% n-SiC	0.05 @ 200 C, 45 MPa	4×10^{-10}	416.66	Ferkel et al. [15]
Mg-9Al-1Zn-25 vol% SiC	0.09 @ 175 C, 80 MPa	0.75×10^{-6}	95.0	Abhilash et al. [34]

dislocation creep. The time-to-fracture for the composites is lengthened by three orders of magnitude relative to pure magnesium.

2. Fractography analysis revealed that while pure magnesium appears to fracture by dislocation slip, the polymer derived MMCs fail from the nucleation and growth of voids at the grain boundaries.
3. The presence of thermally stable SiCNO particles which segregated near to grain boundaries produces highly stable microstructures during creep deformation until fracture mode to become intergranular by void's nucleation and growth.
4. In the longer term, the remarkable high temperature mechanical properties of polymer derived MMCs hold the intriguing possibility of their deployment in automobile engines.

Acknowledgments

This research was supported by the Metals and Nanomaterials program in the Division of Materials Research at the National Science Foundation under Grant No. DMR1105347.

References

[1] B.L. Mordike, T. Ebert, Mater. Sci. Eng. A 302 (2001) 37–45.
[2] H. Friedrich, S. Schumann, J. Mater. Proc. Tech. 117 (2001) 276–281.
[3] D. Amberger, P. Eisenlohr, M. Goken, Mater. Sci. Eng. A 510–511 (2009) 398–402.
[4] M. Rashad, F. Pan, D. Lin, M. Asif, Mater. Des. 89 (2016) 1242–1250.
[5] D.J. Lloyd, Inter. Mater. Rev. 39 (1994) 1–23.
[6] T.M. Pollock, A.S. Argon, Acta Metall. Mater. 40 (1992) 1–30.
[7] M. Gupta, W.L.E. Wong, Mater. Charact. 105 (2015) 30–46.
[8] Sudarshan, K. Terauds, A.R. Anilchandra, R. Raj, Metall. Mater. Trans. A 45 (2014) 551–554.
[9] Sudarshan, M.K. Surappa, D. Ahn, R. Raj, Metall. Mater. Trans. A 39 (2008) 3291–3297.
[10] R. Raj, M.K. Surappa, Sudarshan, United States patent US 8,540,797. 2013 Sep 24.
[11] E. Castellan, G. Ischia, A. Molinari, R. Raj, Metall. Mater. Trans. A 44 (2013) 4734–4742.
[12] A. Kumar, R. Raj, S.V. Kailas, Mater. Des. 85 (2015) 626–634.
[13] N.M. Chelliah, H. Singh, R. Raj, M.K. Surappa, Mater. Sci. Eng. A 685 (2017) 429–438.
[14] N.M. Chelliah, H. Singh, M.K. Surappa, Mater. Chem. Phys. 194 (2017) 65–76.
[15] H. Ferkel, B.L. Mordike, Mater. Sci. Eng. A 291 (2001) 193–194.
[16] F. Labib, R. Mahmudi, H.M. Ghasemi, Mater. Sci. Eng. A 640 (2015) 91–97.
[17] R. Fernandez, G. Gonzalez-Doncel, Mater. Sci. Eng. A 528 (2011) 8218–8225.
[18] T.W. Gustafson, P.C. Panda, G. Song, R. Raj, Acta Mater. 45 (1997) 1633–1643.
[19] R. Raj, R. Riedel, G.D. Soraru, J. Amer. Cer. Soc. 84 (2001) 2158–2159.
[20] E 139-00, Standard test methods for conducting creep, creep-rupture, stress-rupture tests of metallic materials, ASTM Handbook, 2000.
[21] M.F. Ashby, L.M. Brown, Phil. Mag. 8 (1963) 1649–1676.
[22] F.C. Monkman, N.J. Grant, Proceedings of American Society Testing of Materials, vol. 56, eighth ed., 1956, p. 593.
[23] M.W. Toaz, R.E.J. Ripplings, Trans. AIME 206 (1956) 936.
[24] M.F. Ashby, H.J. Frost, Deformation-Mechanism Maps, Pergamon Press, Oxford, 1982.
[25] S.S. Vagarali, T.G. Langdon, Acta Metall. 29 (1981) 1969–1982.
[26] W.M. Tegart, Acta Metall. 9 (1961) 614–617.
[27] F. Dobes, K. Milicka, Met. Sci. 10 (1976) 382–384.
[28] G. Sundararajan, Mater. Sci. Eng. A112 (1989) 205–214.
[29] R. Raj, Acta Metall. 26 (1978) 995–1006.
[30] S.C. Tjong, Z.Y. Ma, Mater. Sci. Eng. R 29 (2000) 49–113.
[31] R. Raj, M.F. Ashby, Acta Metall. 23 (1975) 653–666.
[32] R. Raj, A.K. Ghosh, Metall. Trans A 12 (1981) 1291–1302.
[33] A. Kiełbus, T. Rzychoń, Mater. Sci. Forum 638–642 (2010) 1546–1551.
[34] A. Viswanath, H. Dieringa, K.K. Ajith Kumar, U.T.S. Pillai, B.C. Pai, J. Mag. Alloys 3 (2015) 16–22.